Molecular Therapy
Oncology
Original Article

KPC pancreatic cancer cells are a novel immunocompetent murine model supporting human adenovirus replication and tumor oncolysis

Marc Otero-Mateo,[1] Francesc Estrany Jr,[1,2] Sabrina Arcas-Márquez,[1] Laura Moya-Borrego,[3] Giancarlo Castellano,[1] Miquel Castany,[1] Ramon Alemany,[3] and Cristina Fillat[1,4,5]

[1]Institut d'Investigacions Biomèdiques August Pi i Sunyer (IDIBAPS), 08036 Barcelona, Spain; [2]Programa de Biomedicina. Universitat de Barcelona, 08036 Barcelona, Spain; [3]Cancer Immunotherapy Group, Oncobell and iProCURE Programs, IDIBELL-Institut Català d'Oncologia, 08908 L'Hospitalet de Llobregat, Barcelona, Spain; [4]Centro de Investigación Biomédica en Red de Enfermedades Raras (CIBERER), 08036 Barcelona, Spain; [5]Facultat de Medicina i Ciències de la Salut. Universitat de Barcelona, 08036 Barcelona, Spain

Oncolytic adenoviral therapy is a promising approach for pancreatic cancer treatment. However, the limited capacity of murine cells to produce infectious viral progeny precludes the full evaluation of the virotherapy in a suitable immunocompetent mouse model. Here, we report that the murine KPC-I cell line, established from pancreatic tumors developed in *LSL-Kras*^{G12D}; *LSL-Trp53*^{R172H}; *Pdx-Cre* mice, is susceptible to adenoviral replication and generates a progeny of infective virions similar to those from infected human A549 cells. A comparative study with the semipermissive murine CMT64.6 cells reveals that adenoviral infection of KPC-I cells substantially increases the release of infective particles, with a correlating enhanced susceptibility to adenovirus-induced autophagy. Remarkably, systemic delivery of the oncolytic adenovirus AdNuPARE1A in athymic mice bearing KPC-I tumors results in significant inhibition of tumor growth. Moreover, KPC-I tumors in immunocompetent mice with intratumoral administration of AdNuPARE1A or ICOVIR15kDelE3 display significant antitumoral effects, with evidence of adenoviral replication. Collectively, our data show that KPC-I cells are permissive to human oncolytic adenovirus replication, rendering KPC-I syngeneic tumors an interesting model to evaluate the multifaceted antitumor activities of oncolytic adenovirus.

INTRODUCTION

Oncolytic adenoviruses (OAs) are engineered to selectively replicate and lyse tumor cells. The anticancer effects of OAs result from the combined action of the lytic activity and the stimulation of an immune response. In clinical trials, OAs have already demonstrated efficacy as a monotherapy or in combination with other immunotherapies.[1] Of note, data from the trials highlight that therapeutic efficacy can be improved by facilitating the antitumor immune response. Current efforts in the field rely on a broad number of strategies to engineer OAs with improved immunostimulatory functions.[2] However, in addition to the anticancer immune effects, OA administration also triggers an anti-viral response, and the balance between the two immunities needs to be studied to identify optimal candidates for clinical development.

Thus, the immunobiological effects of new-generation OAs should be analyzed in reliable preclinical models. Syrian hamsters have been used to study OAs, as they are partially permissive to human adenovirus species C replication, the most common adenoviral species in virotherapy studies.[3] However, the limited availability of reagents, as well as the complexity of animal housing and manipulation, reduces the utility of Syrian hamster models. The possibility of using immunocompetent mouse models to study OA antitumor efficacy has been hindered by the limited ability of human adenovirus to replicate in murine cells. Early studies showed that adenoviruses replicate 1,000-fold lower in mouse cells than in human cells.[4] More recently, a few murine cell lines of ovarian and lung cancer origin have been identified that are minimally permissive to human adenoviral replication.[5–8] A failure of efficient protein synthesis, with reduced loading of mRNAs (and especially late mRNAs) onto ribosomes, has been proposed as a mechanism underlying the limited productive adenoviral infection in murine cells.[9]

Here, we demonstrate that KPC-I cells derived from a murine pancreatic cancer model are permissive to adenoviral replication. We show that viral protein synthesis, and especially viral progeny release, is significantly enhanced in KPC-I cells with respect to other murine cancer cells. We used bulk RNA sequencing (RNA-seq) analysis to identify a subset of genes that are deregulated in response to adenoviral infection, which highlights the pivotal roles of calcium signaling and autophagy. Further, our data suggest that the permissiveness of KPC-I cells to OAs is related to a higher susceptibility of KPC-I cells

Received 1 August 2024; accepted 18 December 2024;
https://doi.org/10.1016/j.omton.2024.200928.

Correspondence: Cristina Fillat, Institut d'Investigacions Biomèdiques August Pi i Sunyer (IDIBAPS), 08036 Barcelona, Spain
E-mail: cfillat@recerca.clinic.cat

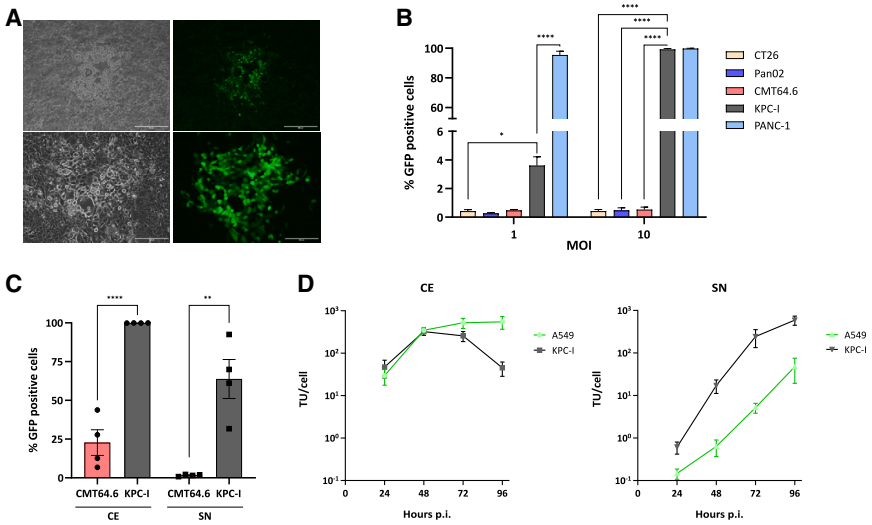

Figure 1. KPC-I cells produce infective viral progeny

(A) Representative images of plaque formation after infection with the Adwt-E, showing bright-field (left) and GFP fluorescence (right). (B) Viral release from the supernatant (SN) of the indicated cell lines infected with Adwt-E at 1 or 10 MOI for 72 h. A fraction of the SN was used to infect A549 cells, and the percentage of GFP-positive cells was quantified after 30 h. (C) Production of infective particles that were released (SN) or in intracellular cell extracts (CEs) from CMT64.6 and KPC-I cells infected with Adwt-E at 100 MOI for 48 h. A fraction of the SN or CE was used to infect A549 cells, and the percentage of GFP-positive cells was quantified after 30 h. (D) Viral production. A549 or KPC-I cells were infected with Adwt-E at 30 or 100 MOI, respectively, and CEs and SNs were harvested at the indicated time points and titrated. Data are expressed as the means ± SEM of n = 3–5 independent replicates. Significance was assessed using a two-tailed Mann-Whitney test. $^{*}p < 0.05$, $^{**}p < 0.01$, and $^{***}p < 0.001$.

to autophagy-mediated cell lysis. Critically, we show that OAs can trigger antitumor effects in KPC-I tumors in the context of both immunodeficient and immunocompetent mice.

RESULTS

Murine KPC-I cells are susceptible to human adenovirus infection

Human adenovirus type 5 (Ad5) replicates poorly in murine cells, and this limits the evaluation of OA efficacy in immunocompetent models. We studied the susceptibility of the murine pancreatic cancer cell line KPC-I, established from spontaneous pancreatic tumors of 20-week-old, genetically engineered *LSL-Kras*^{G12D}; *LSL-Trp53*^{R172H}; *Pdx-Cre* (KPC) mice,[10] to Ad5 infection. KPC-I cells grow as monolayer cultures of epithelial morphology and maintain the genetic mutations *Kras*^{G12D} and *Trp53*^{R172H} (Figures S1A and S1B).

We first analyzed their susceptibility to adenoviral transduction. KPC-I cells were transduced with the non-replicative adenoviral vector AdTL(AdTrack-Luc) that expresses the green fluorescence protein (GFP) at different multiplicity of infection (MOI) levels (Figure S2A).[11] Flow cytometry analysis of GFP-positive cells showed close to 100% infectivity when cells were transduced at 100 MOI (Figures S2B and S2C). At this viral dose, the murine lung carcinoma cell line CMT64.6 was transduced at similar levels, but the murine cancer cells CT26 and Pan02 displayed very low levels of adenoviral transduction (Figure S2B). The human pancreatic cancer cell line PANC-1 was about 10 times more susceptible to adenoviral transduction than KPC-I or CMT64.6 cells[12] (Figure S2B). Expression analysis by flow cytometry revealed that the coxsackie adenovirus receptor (CAR) was expressed at high levels in PANC-1 cells but at similar lower levels in both KPC-I and CMT64.6 cells (Figure S3). Likewise, expression of the integrin β3 showed a similar percentage (from 99% to 100%) of positive cells in KPC-I and CMT64.6 cells, while integrin αv was slightly lower expressed in CMT64.6 cells (Figure S3). Analysis of the cell surfaces of the KPC-I, CMT64.6, and PANC-1 cells revealed strong expression of desmoglein-2 (DSG2) in all three cell lines (Figure S3). As DSG2 has been identified as the primary high-affinity receptor used by the adenoviruses Ad3, Ad7, Ad11, and Ad14, these results suggest potential susceptibility of these cell lines to adenoviral transduction with the indicated serotypes, and even to chimeric serotypes, such as the commonly used Ad5/3, expanding their value in the OA field.[13] Altogether, these results show that the murine cell lines KPC-I and CMT64.6 uptake adenoviral particles in a similar manner.

Murine KPC-I cells are permissive to human adenovirus replication

Next, we assessed the permissiveness of KPC-I cells for adenovirus replication. We infected KPC-I cells with the replication-competent adenovirus Adwt-E (which expresses enhanced GFP as a late gene) and performed a plaque assay. We observed lysis plaques surrounded by cytopathic cells expressing GFP in different regions of the wells, revealing the capacity of the virus to replicate and infect neighboring cells (Figure 1A). We then compared the replication capacity of KPC-I cells to the murine cell lines CMT64.6 (which was previously described as semipermissive to adenoviral replication[5]), CT26, and Pan02. As a positive control, we used the human cell line PANC-1, known to be highly permissive to adenoviral replication, similar to A549 cells.[14,15] Briefly, we infected cells with 1 or 10 MOI for 72 h, used the supernatants as the source of virus to infect A549 cells for 30 h, and then determined the GFP-positive cells. We only detected GFP expression in A549 cells that had been exposed to supernatant from PANC-1 or KPC-I cells, suggesting that there was no virus production in the murine CMT64.6, Pan02, or CT26 cell lines (Figure 1B). For Pan02 and CT26 cells, the absence of viral production could be partially related to the low infectivity at the MOI used. However, other factors are likely involved in the resistance of CMT64.6 cells, as KPC-I and CMT64.6 cells displayed similar susceptibility to adenoviral transduction (Figures S2B and S2C). Permissiveness to adenoviral replication was also observed in KPC-II cells derived from a different KPC tumor, suggesting that KPC cell lines have a

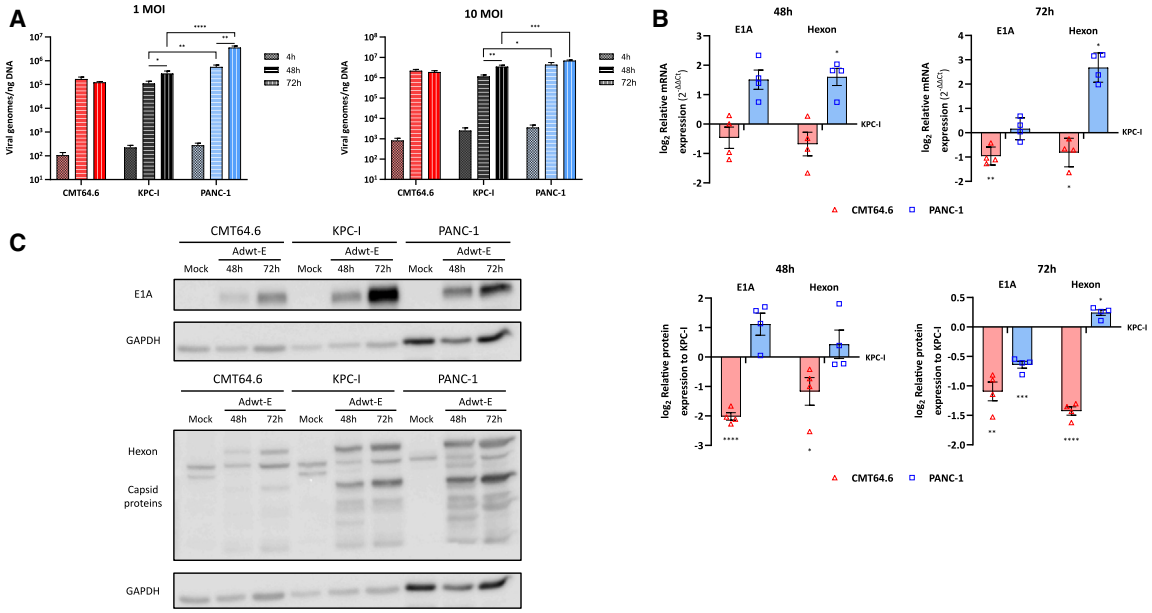

Figure 2. Characterization of the intracellular steps of Adwt-E viral infection in CMT64.6 and KPC-I cells

(A) Entry and viral genome replication quantification in CMT64.6, KPC-I, and PANC-1 cells infected with 1 or 10 MOI of Adwt-E for 4, 48, or 72 h. Viral genomes were quantified by qPCR of the L3 region. (B) Relative viral E1A and hexon mRNAs analyzed by RT-qPCR in CMT64.6 and KPC-I cells infected with 10 MOI of Adwt-E for 48 or 72 h. CMT64.6 and PANC-1 results are expressed relative to KPC-I. (C) E1A and capsid viral proteins expression by western blot in CMT64.6, KPC-I, and PANC-1 cells infected with 10 MOI of Adwt-E for 48 or 72 h. Quantification of E1A and hexon protein levels are expressed as relative to KPC-I. Data are expressed as the means ± SEM of $n = 4$ independent replicates. Significance was assessed using a two-tailed Mann-Whitney test. $^{*}p < 0.05$, $^{**}p < 0.01$, and $^{***}p < 0.001$.

comparable response to adenoviral infection (Figure S4). To further study the susceptibility to viral replication, we tested the KPC-I and CMT64.6 cells in a virus production assay. We infected both cultures with Adwt-E at an MOI that resulted in 90%–100% of infection. At 48 h post-infection, the cell extracts (CEs) and supernatants were used to infect A549. We observed significantly more GFP-positive A549 cells in both the CE (4-fold) and supernatant (40-fold) from KPC-I cells as compared to those from CMT64.6 cells, indicating that KPC-I cells were much more permissive to adenoviral replication (Figure 1C). Of note, the degree of replication and the kinetics of viral production in KPC-I cells were similar to those of the reference human cell line A549. Strikingly, the extracellular component (i.e., the supernatant) from KPC-I cells contained about 5 times more infective viral particles than that from A549 cells, suggesting a higher viral release in KPC-I cells (Figure 1D).

KPC-I cells are susceptible to adenovirus-mediated cell lysis by autophagy

To further characterize the supportive adenoviral replication activity in KPC-I versus CMT64.6 cells, we analyzed whether differences between the two cell lines were related to the capacity of the viral genome to replicate inside the cells. We discarded the CT26 and Pan02 cells due to their limited susceptibility to adenoviral transduction, and we used PANC-1 cells as a human cellular model. We assessed for genome replication in cells infected with Adwt-E at 1 or 10 MOI and analyzed for the presence of intracellular genomes over time (at 4, 48, and 72 h). We detected similar numbers of genomes in the two murine cell lines at 4 h, indicating equivalent viral entry. The number of genomes was also similar between the murine cell lines at 48 h, suggesting similar genome replication. At 72 h post-infection, significantly higher viral genomes were observed when compared to those at 48 h in KPC-I cells at the two MOI tested and in PANC-1 when infected at 1 MOI, suggesting secondary infections in these cells. In all the conditions, the viral genomes were significantly lower in the murine cell lines than in human PANC-1 cells (Figure 2A). We then examined the expression of early and late genes at the transcriptional level. At 10 MOI, both the *E1A* and *L3* (hexon) genes were similarly transcribed in infected CMT64.6 (CMTI) and infected KPC-I (KPCI) cells at 48 h. At 72 h, we observed significant differences in the mRNA expression of the two viral genes between cell lines, probably because of the secondary infections occurring in KPC-I cells, when infected at 10 MOI (Figure 2B).

Previous studies on Ad5 replication in murine cells have shown the failure of late protein expression.[9] We observed higher expression of E1A (an early protein) and the structural viral proteins (late proteins) in KPCI cells as compared to CMT64.6 cells at the two time points analyzed.

PANC-1 cells showed higher mRNA viral transcripts and protein content at 48 h with respect to KPC-I cells (Figures 2B and 2C). However, at 72 h, the contents of E1A transcripts in PANC-1 and KPC-I cells were similar (Figure 2B). This may be related to differences in the viral kinetics between cell lines as well as secondary infections

occurring in KPC-I cells but not in PANC-1 cells when they were infected at 10 MOI. Adwt-E expresses GFP as a late gene; similar to what we observed for the viral proteins, GFP expression was much lower in CMT64.6 cells at 48 h post-infection (Figure S5). Altogether, these results showed that CMT64.6 and KPC-I cells displayed similar levels of infectivity, genome replication, and viral mRNA transcription but that protein expression of both early and late proteins was more efficient in KPC-I cells.

To gain further insight into the mechanisms that support adenoviral replication in murine KPC-I cells, we designed a transcriptomic study in which we infected KPC-I and CMT64.6 cells with 100 MOI of Adwt-E and then performed bulk RNA-seq at 40 h post-infection. Mock KPC-I cells, untransduced KPC-I (KPCU), and KPCI cells clustered together and differently than mock CMT64.6 cells, untransduced CMT (CMTU), or CMTI cells, highlighting intercellular variability (Figure 3A). We observed transcriptional differences between mock- and adenoviral-infected cells in both cell lines (Venn diagram, Figure 3B). Differential gene transcriptional changes triggered by infection between cell lines displayed a set of 1,353 deregulated genes ($p < 0.05$). Gene Ontology (GO) analysis identified terms related to ion transport and calcium signaling, with a signature of 24 downregulated genes (Figures 3C–3E). Several of these genes were validated by RT-qPCR, confirming the RNA-seq data and showing that CMTI cells, but not KPCI cells, had a trend of a significantly upregulated subset of genes (Figure 3F). Notably, several of these genes were related to autophagy processes. Gene set enrichment analysis (GSEA) identified enrichment of genes grouped in the GO term autophagy (Figure 3G). Previous reports have shown that human Ad5 induces cell lysis through autophagy.[16] We investigated the autophagy response to adenoviral infection in KPC-I and CMT64.6 cells by analyzing the conversion of LC3-I to LC3-II at 32, 48, and 72 h after viral infection. We only observed upregulation of LC3-II in KPCI cells, indicating that the autophagy cascade was activated in KPC-I cells but not CMT64.6 cells. In line with this, the levels of the p62 protein, which is degraded through autophagy, decreased in KPCI cells at the latest time point (72 h) (Figure S6A). We observed similar results in the human PANC-1 cell line following adenoviral infection (Figure S6B). Furthermore, adding 3-methyladenine (3-MA), an inhibitor of autophagy initiation, to adenovirus-infected KPC-I or CMT64.6 cells diminished the viral progeny release only in KPC-I cells (Figure 4B). The lack of autophagy induction upon adenoviral infection in CMT64.6 cells correlates with the low release of infective adenoviral particles (Figures 1B, 1C, and 4B). These results are in line with previous observations demonstrating that autophagosome formation is sufficient to disrupt the integrity of the cell membrane, contributing to cell lysis and viral spread.[16]

OAs trigger antitumor activity in KPC-I tumors generated in either nude or immunocompetent mice

Next, we assessed the susceptibility of KPC-I cells to OA killing. For this, we tested the oncolytic activity of the AdNuPARE1A virus, previously generated in our laboratory.[17,18] AdNuPARE1A induced KPC-I cytotoxicity in a dose-dependent manner, with 100% cell death at 100 MOI. KPC-I cells displayed higher sensitivity to adenoviral cell killing than CMT64.6 cells, in line with their higher replication permissiveness. The human PANC-1 cell line was more sensitive to adenoviral cell death (Figure 5A). The oncolytic effects in KPC-I were also observed with the OA ICOVIR15kDelE3, although AdNuPARE1A displayed increased potency (Figure 5B).

To determine the ability of AdNuPARE1A to control tumor growth *in vivo*, KPC-I cells were subcutaneously implanted into the flanks of nude mice, and then the mice were treated with 5×10^{10} viral particles (vp)/mouse intravenously. AdNuPARE1A controlled tumor growth in a 20 day follow-up, consistent with the susceptibility of KPC-I cells to adenoviral lysis (Figure 5C). Expression of E1A in the tumors at 20 days after viral administration further indicated the presence of replicating active virus (Figure 5D). However, the control of tumor growth was less pronounced than in PANC-1 xenografts, as suggested from previous experiments.[15] This could be explained by the lower infectivity of KPC-I as compared to PANC-1 (10-fold), which could diminish the spread of the virus within the tumor.

Given the antitumor effects observed in KPC-I tumors in nude mice, we next explored the efficacy of AdNuPARE1A and ICOVIR15kDelE3 in the more challenging setting of immunocompetent mice. To partially overcome the limited infectivity, we performed intratumor administration of 1×10^{11} vp/tumor three times (on days 15, 18, and 22) for KPC-I tumors generated in C57BL/6J immunocompetent mice; we monitored tumor growth for up to 31 days. Both AdNuPARE1A and ICOVIR-15kDelE3 displayed similar antitumor efficacy (Figure 6A). At day 31, the E1A and hexon mRNAs were detected in AdNuPARE1A-treated tumors, indicating the presence of an actively replicating adenovirus (Figure 6B). Hexon mRNA was also detected in ICOVIR15kDelE3-treated tumors but at significantly lower levels than in the AdNuPARE1A-treated tumors (Figure 6B). We observed a similar trend when the viral genomes were quantified (Figure 6C). Moreover, we found that tumors treated with either virus produced infective viral progeny, further demonstrating the permissiveness of KPC-I cells to Ad5 OA replication (Figure 6D). Strikingly, AdNuPARE1A treatment induced a significant and efficient increase in the mRNA levels of interferon (IFN)-γ and granzyme B, suggesting the activation of tumor infiltrates (Figure 6E).

Altogether, the results of this study show that KPC-I cells support human Ad5 replication, in part due to an enhanced release of adenoviral progenies. OAs in KPC-I tumors are capable of controlling tumor growth in nude mice when delivered systemically. Importantly, intratumor administration in immunocompetent mice led to remarkable antitumor efficacy. Thus, these results point to KPC-I cells as a good model to study adenoviral-mediated antitumor responses and evaluate the potential of combination with immunotherapies.

DISCUSSION

OA therapies are envisioned as attractive therapeutic modalities against cancer. Even though clinical trials are already ongoing, special efforts are needed to act against instances of neoplasia that have a

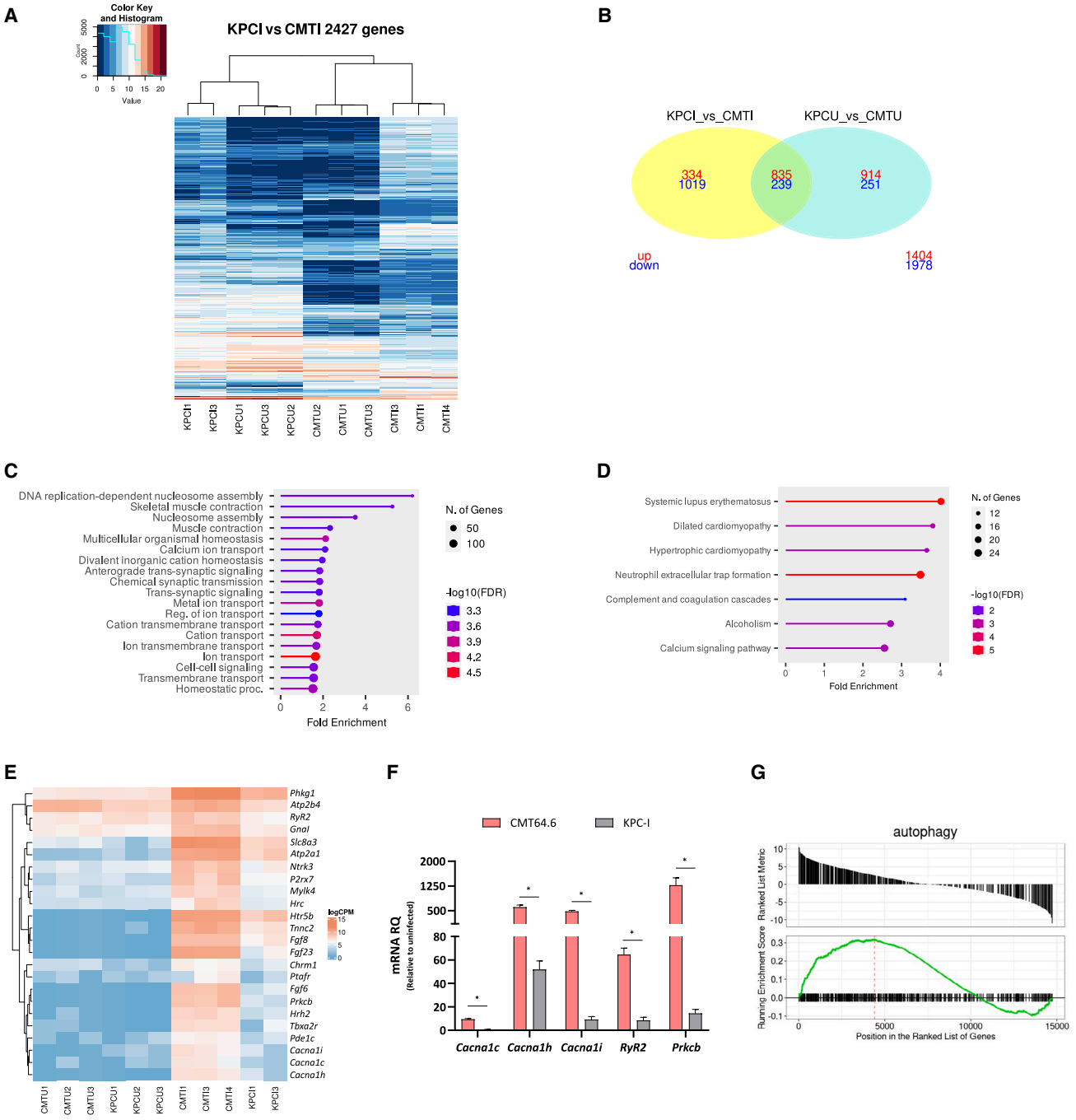

Figure 3. Transcriptional profile of KPC-I and CMT64.6 cells infected with Adwt-E

(A) Unsupervised clustering of gene expression profiles based on differentially expressed genes between KPCI versus CMTI cells. Significantly differentially expressed genes are considered those with $\log_2$-fold change (FC) > 2 and $p < 0.05$. (B) Venn diagram showing the distribution of deregulated genes in the indicated comparisons. (C) Gene Ontology enrichment analysis was performed using ShinyGO (v.0.80) for the 1,353 differentially expressed genes (D) or the 1,019 downregulated genes in infected cells. (E) Heatmap showing the gene clustering of the selected gene list corresponding to the GO term calcium signaling pathway. (F) qPCR assessment of genes associated with calcium signaling. Data are expressed as the means ± SEM of $n = 4$ independent replicates. Significance was assessed using a two-tailed Mann-Whitney test. *$p < 0.05$, **$p < 0.01$, and ***$p < 0.001$. (G) GSEA plot showing enrichment of autophagy-related genes.

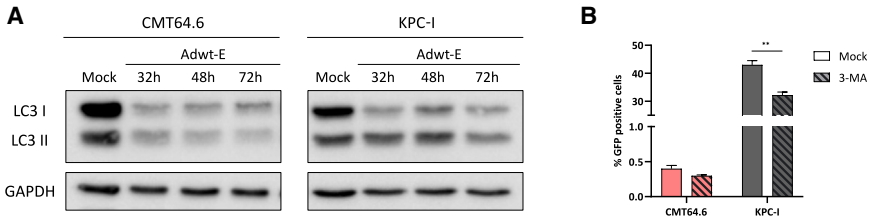

Figure 4. Adwt-E induces the expression of autophagic marks in KPC-I cells

(A) CMT64.6 and KPC-I were infected with Adwt-E at 100 MOI. Cells were harvested at 32, 48, and 72 h post-infection, and LC3 I and LC3 II protein expression levels were measured by western blot. GAPDH detection was used as loading control. Representative western blots of $n = 3$ independent experiments are shown. (B) Viral release from the supernatant (SN) of KPC-I and CMT64.6 cells infected with Adwt-E at 5 MOI for 72 h in the presence or absence of 1 mM 3-methyladenine (3-MA). A fraction of the SN was used to infect A549 cells, and the percentage of GFP-positive cells was quantified after 30 h.

poor response to current therapies. This is the case of pancreatic ductal adenocarcinoma, which currently is ranked the third-most cause of cancer deaths and is expected to be the second-most cause by 2030.[19,20] To date, the efficacy of OA therapies against pancreatic tumors mostly relies on xenograft models in nude mice, which, however, preclude the contribution of the immune system.[21–23] The lack of a murine model that allows for efficient adenoviral replication has been a strong limitation in the OA field and has hindered the evaluation of their full potential that results from the combined effects of the cytolytic activity and the antitumor immune response. Here, we provide evidence that adenoviral replication in KPC-I murine pancreatic cancer cells induces cell lysis, likely mediated by a higher susceptibility to adenovirus-induced autophagic cell death. We also demonstrate *in vivo* oncolytic tumor growth control of AdNuPARE1A and ICOVIR15kDelE3 in KPC-I tumors in nude and immunocompetent mice.

The species restriction of human Ad5 replication is not absolute, but clearly there is a failure in the efficient productivity of new infective progenies in most of the murine cells tested. In this study, we show that KPC-I cells, derived from tumors bearing $Kras^{G12D}$ and $Trp53^{R172H}$ mutations, support adenoviral replication and cytolysis induction. Interestingly, the levels of viral production and viral release by KPC-I cells were close to what has been observed in human cells. However, viral entrance was highly diminished in KPC-I cells, being at least 10-fold lower than that in human PANC-1 cells, a cell line highly susceptible to adenoviral infection. This could be related to the limited expression of CAR in these cells, which could be mitigated by engineering KPC-I cells with human CAR (hCAR) to facilitate transduction. Nonetheless, viral entrance was independent of adenoviral replication. In fact, KPC-I cells displayed similar viral uptake to the murine CMT64.6 cells.

Even though the CMT64.6 cell line has been reported to be semipermissive,[5] we observed poor adenoviral replication in these cells as compared to KPC-I cells, with reductions in intracellular levels (4-fold) and especially in the release of infective particles (40-fold). The relative blocking of viral replication was not attributable to viral genome replication nor to viral gene transcription but rather (at least in part) to viral protein expression. Our data are in line with previous studies showing a failure of translation of human adenovirus mRNA in murine cancer cells due to poor recruitment to ribosomes.[9] We also observed that protein translation was significantly more impaired in CMT64.6 cells.

Notably, the KPC-I and CMT64.6 cell lines present different mutational landscapes: while both have *K-Ras*-activating mutations, CMT64.6 has wild-type *Trp53*, but KPC-I carries the $Trp53^{R172H}$ mutation (the mouse ortholog to the human $TP53^{R175H}$).[24] p53 regulates a vast range of functions, and wild-type and mutant p53 often have opposing roles, generating very complex and diverse scenarios.[25] Thus, the divergency in the *Trp53* status, and other potential mutations in each cell line, creates a singular genetic background that could determine the response to adenoviral infection.

Even though E1A expression was lower in CMTI cells than in KPCI cells, it was sufficient to enable similar levels of viral DNA replication in both lines, demonstrating that even a low E1A level can facilitate viral cycle progression. The reduced expression of late proteins probably explained the diminished viral production determined in CEs of CMT64.6 cells when compared to KPC-I cells. However, the major impairment in CMT64.6 cells was observed in the release of the infective particles, whereas KPC-I displayed a viral release similar to human cells. Our transcriptomic study comparing the response of each cell line to adenoviral infection pointed to a set of differentially regulated genes, enriched in GO terms of cation transport, ion transmembrane transport, and calcium signaling pathway. These terms fit with the concept that viruses use calcium components to elevate cytosolic calcium concentrations, which then activate Ca^{2+}-dependent/sensitive enzymes and transcriptional factors, in turn promoting the viral cycle. This suggests that an imbalance in the genes participating in these processes may alter viral replication.[26] We identified an autophagic gene set enrichment and could demonstrate that an autophagy-mediated cell death occurred in KPC-I cells, but not in CMT64.6 cells, upon adenoviral infection. Importantly, treatment of KPC-I cells with the autophagic inhibitor 3-MA, which regulates autophagic sequestration, reduced viral release from KPCI cells. Autophagy correlates with cell lysis induced by the virus, and it has been demonstrated that autophagosome formation is sufficient to disrupt the integrity of membrane structures in cells, allowing infective virions to be released.[16] The impaired induction of autophagy in CMTI cells that we observed is in line with the small fraction of infective virions released from CMT64.6 cells as compared to KPC-I cells.

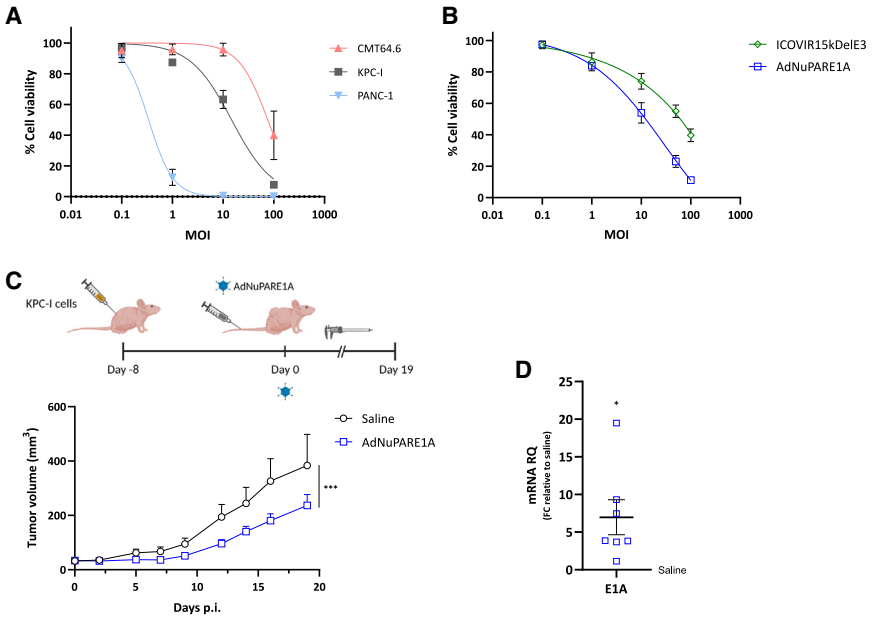

Figure 5. Oncolytic AdNuPARE1A controls tumor growth in KPC-I tumors in nude mice

(A) *In vitro* cytotoxicity assay of AdNuPARE1A. KPC-I, CMT64.6, and PANC-1 cells were infected with AdNuPARE1A at the indicated doses, and cell viability was assessed 5 days after infection. Data are expressed as the means ± SEM of $n = 4$ independent replicates. (B) Comparative *in vitro* cytotoxicity of AdNuPARE1A and ICOVIR15kDelE3. KPC-I cells were infected with the indicated viruses at doses from 0.1 to 100 MOI, and cell viability was assessed at 4 days after infection. Data are expressed as the means ± SEM of $n = 4$ independent replicates. (C) Antitumor study. Nude mice bearing subcutaneous KPC-I tumors were intravenously injected with saline or 5×10^{10} vp/mouse of AdNuPARE1A. Follow-up of tumor growth is represented as the mean of tumor volume ± SEM ($n = 12$). (D) qPCR analysis of E1A mRNA levels at day 20. mRNA values are expressed relative to the *Hprt1* and as fold changes relative to saline-injected tumors. Each dot represents an individual tumor ($n = 5$–7). Data are expressed as the means ± SEM. Significance was assessed using a two-tailed Mann-Whitney test. $^{*}p < 0.05$, $^{**}p < 0.01$, and $^{***}p < 0.001$.

Several deregulated genes have been proposed to be involved in the autophagic process. The calcium voltage-gated channels Cacna1c, -1h, and -1i were induced upon infection in CMT64.6 cells but not KPC-I cells. Calcium channels mediate ion fluxes across cellular membranes and are regulators of both basal and induced autophagy. However, the mechanisms by which specific ion channels regulate autophagy are complex, with both stimulatory and inhibitory functions.[27] Calcium influx through voltage-gated calcium channels can inhibit autophagy and silence the L-type CACNA1C/Cav1 and CACNA1D/Cav1.3 channels, resulting in an accumulation of LC3-II.[27] Moreover, Ca^{2+} channel blockers induce autophagy due to the loss of autophagy-suppressing Ca^{2+} signals.[28] Verapamil, a Cacna1c blocker, substantially enhances the cellular release of infective adenovirus.[29] Based on this, we can speculate that the upregulation of calcium voltage-gated channels in CMTI cells permits an increased influx of calcium-inhibiting adenovirus-induced autophagy.

The ryanodine receptor type 2 (RyR2) is another calcium channel that was upregulated in CMTI cells but not KPCI cells. RYRs are endoplasmic reticulum (ER)-located calcium-permeable channels that mediate the release of calcium from internal stores. The role of RYRs in autophagy has been much less studied than those of other calcium channels.[30] For instance, depletion of RYR2 reduces mitochondrial calcium levels and increases autophagy in cardiomyocytes.[31] On the other hand, increased RYR2 activity in a model of Alzheimer disease inhibits autophagy.[32] Thus, we could speculate that the upregulation of RYR2 in CMTI cells could contribute to interfering with adenovirus-induced autophagy.

Finally, another molecule involved in autophagy that showed major changes in expression between CMT64.6 and KPC-I cells upon infection was protein kinase C β (PRKCB), a member of the classical PRKCs. Activation of PRKCB negatively modulates the mitochondrial energy status and inhibits autophagy, and its overexpression inhibits chemotherapy-induced autophagy.[33,34] These genes are some examples of potential actors that help to understand the different behaviors of CMT64.6 and KPC-I cells. However, many of the other genes identified in the GSEA under the GO term autophagy might also contribute. Thus, our study has identified a set of genes that participate in the host response to adenoviral infection in CMT64.6 and KPC-I cells, which could impact adenovirus-induced autophagy with implications in viral release.

Of note, our study also shows that treating KPC-I tumors with OAs, either systemically or intratumorally, controlled tumor growth in both nude and immunocompetent mice. Furthermore, we demonstrated that the antitumor activity could be observed using two oncolytic viruses with different backbones, the AdNuPARE1A and the ICOVIR15kDelE3. AdNuPARE1A showed more efficient replication *in vitro*. *In vivo*, we detected virions at 10 days after intratumor administration in the immunocompetent setting. Even though only very low levels of virions were detected in ICOVIR15kDelE3-treated tumors, injection with either virus triggered antitumor efficacy, suggesting that the presence of the virus during the first days post-administration might be sufficient to control tumor size.

The KPC-I model opens the possibility of additional studies, as it integrates the full potential of oncolytic viral activity that results from cytolysis and the antitumor immune response. One could envision studies on OAs that incorporate immunomodulatory transgenes or the evaluation of combination therapies based on OAs with immune checkpoint inhibitors. Some of these strategies have already been

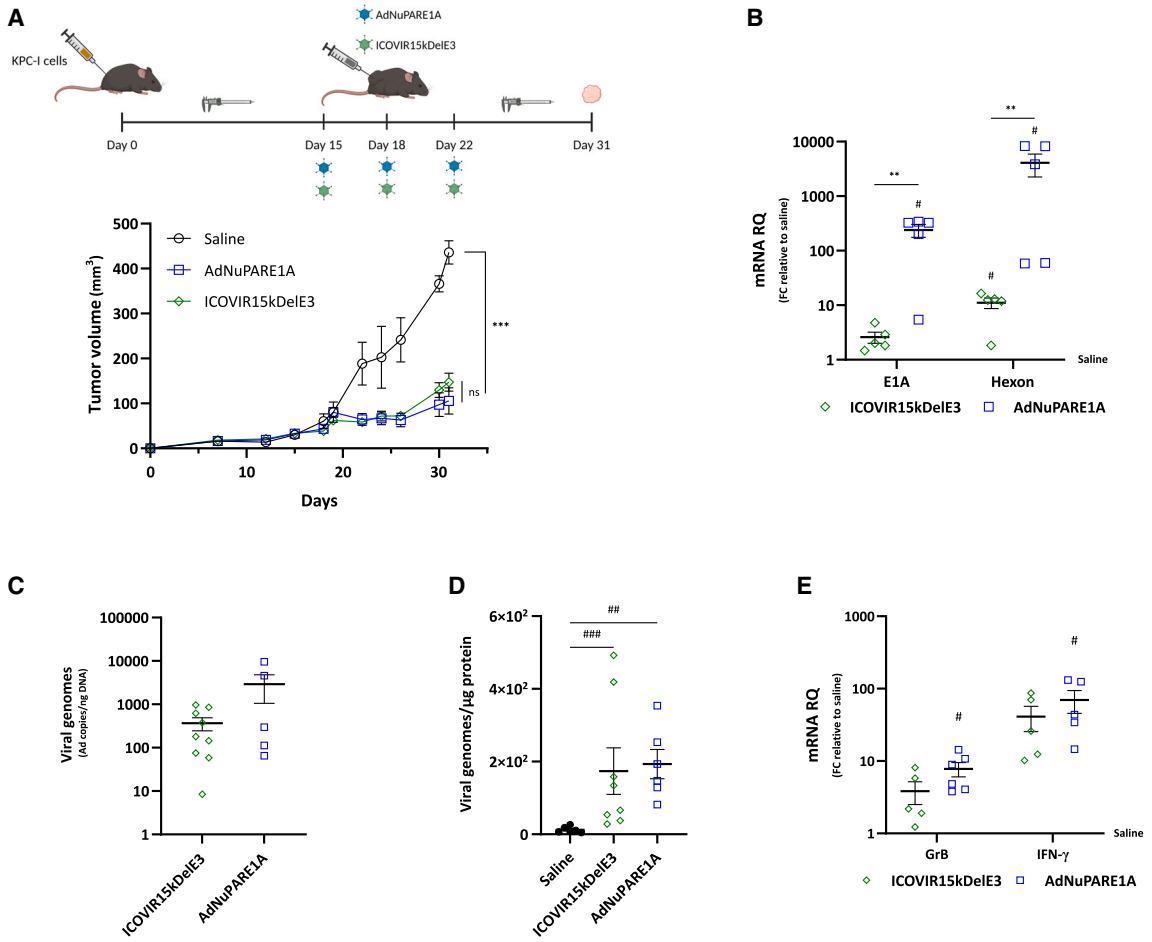

Figure 6. Antitumor efficacy of AdNuPARE1A and ICOVIR15kDelE3 in KPC-I tumors generated in immunocompetent mice

(A) C57BL/6J mice bearing subcutaneous KPC-I tumors were intratumorally administered with saline, AdNuPARE1A, or ICOVIR15kDelE3, at 1×10^{11} vp/tumor, on days 15, 18, and 22. Follow-up of tumor growth is represented as the mean of tumor volume ± SEM (n = 10). *$p < 0.05$, **$p < 0.01$, and ***$p < 0.001$. (B) qPCR analysis of E1A and Hexon mRNA levels at day 31. mRNA values are expressed relative to the *Hprt1* and as fold change relative to saline tumors. Each dot represents individual tumors (n = 5). Data are expressed as the means ± SEM. * indicates significance between tumors receiving saline and virus-treated tumors, # indicates significance between AdNuPARE1A- and ICOVIR15kDelE3-treated tumors. (C) Viral genomes were quantified by qPCR of the L3 region. Values are expressed relative to nanogram of DNA. Each dot represents individual tumors (n = 6–9). Data are expressed as the means ± SEM. (D) Viral genomes in A549 cells infected with supernatants from lysates of the indicated tumors. Values are expressed as the means ± SEM of viral genomes relative to the albumin gene and relative to µg of protein. (E) qPCR analysis of granzyme B and IFN-γ mRNA levels at day 31. mRNA values are expressed relative to the *Hprt1* and as fold change relative to saline tumors. Each dot represents individual tumors (n = 5 or 6). Data are expressed as the means ± SEM. Significance was assessed using a two-tailed Mann-Whitney test. *$p < 0.05$, **$p < 0.01$, and ***$p < 0.001$.

tested in inefficient models, with relatively good responses.[35,36] However, the lack of the lytic effect mediated by the oncolytic virus in the murine models tested likely minimized the achievements. Thus, the KPC-I model described in the current study represents a more clinically relevant model of human cancer to test OA therapies, with added value for the translational perspective.

MATERIALS AND METHODS

Cell lines

Human cell lines A549 (lung carcinoma) and PANC-1 (pancreatic carcinoma) were obtained from the American Type Culture Collection (ATCC, Manassas, VA, USA). The murine cell line CT26 (colorectal carcinoma) was obtained from the ATCC; Pan02 was obtained from CLS Cell Lines Service (Cytion, Germany); CMT64.6, a clone derived from CMT64 cells (lung carcinoma), was obtained by clonal isolation and testing for sensitivity to adenoviral infection,[5] kindly provided by Dr. Ramon Alemany (ICO-IDIBELL, Barcelona, Spain); and KPC-I (pancreatic adenocarcinoma) cells were derived from a KPC mouse tumor established by Dr. Eva Vaquero (IDIBAPS-Hospital Clínic, Barcelona, Spain).[10] All cell lines were routinely tested for interspecies contamination. All cells were grown in Dulbecco's modified Eagle's complete medium supplemented with 10% fetal

bovine serum, L-glutamine (2 mM), penicillin (100 U/mL), and streptomycin (100 μg/mL) and maintained at 37°C in a humidified atmosphere at 5% CO_2.

Adenoviruses

Adenoviruses used in the study were AdTL, a replication-defective adenovirus that expresses the GFP and the luciferase genes under the control of the cytomegalovirus (CMV) promoter[11]; the replication-competent adenovirus Adwt-E (an Ad5wt that expresses enhanced GFP as a late gene)[21]; and the OAs AdNuPARE1A, which incorporates an urokinase-type plasminogen activator receptor (uPAR) minimal promoter and 3× sequence-paired CSL-binding sites (SPS) sequences that recognize the binding domain of the CSL transcription factor characteristic of Notch-responsive genes, regulating E1A transcription,[18] and ICOVIR15kDelE3, which has a deletion of the E3 gene in the ICOVIR15k backbone.[37] Adenoviruses were amplified in HEK293 E1-transcomplementing cells (for AdTL) or A549 cells (for Adwt-E, AdNuPARmE1A, and ICOVIR15kDelE3) and purified by cesium chloride density gradient ultracentrifugation according to standard techniques. Titration of the resulting viral particle concentrations was determined by optical density measurements at 260 nm (OD260) and infective particle units, as previously described.[38]

Reagents

3-MA was obtained from Sigma-Aldrich (St. Louis, MO, USA).

GFP quantification

GFP fluorescence from adenovirus-infected cells was assessed by flow cytometry on a BD LSRFortessa Cell Analyzer 4L (BD Biosciences, Franklin Lakes, NJ, USA).

Flow cytometry analysis of CAR, integrins, and DSG2

For CAR expression analysis, 3×10^4 KPC-I, KPC-II, CMT64.6, or PANC-1 cells were washed once with PBS and then incubated for 30 min at 4°C with the polyclonal CAR antibody, PE Conjugated (bs-2389R-PE; Bioss, Woburn, MA, USA). For αv and β3 integrin expression analysis, 3×10^4 KPC-I, KPC-II, or CMT64.6 murine cells were incubated with a monoclonal antibody, anti-CD51-PE, or anti-CD61-APC (BioLegend, San Diego, CA, USA) for 30 min at 4°C. For DSG2 expression analysis, the indicated cell lines (at a concentration of 3×10^4) were incubated with the DSG2 antibody (F-8) Alexa Fluor 488 sc-365856 (Santa Cruz).

Samples were analyzed using the LSRFortessa Cell Analyzer 5L (BD Biosciences) and FACSDiva software (BD Biosciences).

Plaque assay

KPC-I cells were seeded into 6-well plates at 2×10^5 cells/well. After 16 h, cells were infected with serial dilutions of Adwt-E. At 4 h after infection, the medium was removed, and cells were washed three times with PBS. A 1:1 (DMEM 10% FBS:1% agarose) solution was added to the cells, and, once the agarose overlay had solidified, another layer was added of fresh DMEM (10% FBS). Images were obtained on the indicated day.

Viral production and release kinetics

Cell lines were seeded into 24-well plates at 5×10^4 cells/well and infected with 1 or 10 MOI. At 4 h after infection, cells were washed three times with PBS and incubated with fresh medium. The supernatant containing viral particles was collected after 72 h. A fraction of each supernatant was used to infect A549 cells, and the percentage of GFP was quantified 30 h later. In the studies with KPC-I, CMT64.6, or A549, cells were infected at an MOI that allowed >90% of infection. Viral particles from the supernatants and CEs were collected in triplicate at different time points after infection and titrated in A549 cells.

Cell viability assay

Cells were seeded in 96-well plates at 5×10^3 cells/well and infected with AdNuPARE1A or ICOVIR15kDelE3 at the indicated MOI. At the indicated time points, cell viability was measured using an MTT assay (Thermo Fisher Scientific, Waltham, MA, USA), according to the manufacturer's protocol.

Western blot analysis

Protein extracts were obtained in a lysis buffer (50 mM Tris-HCl [pH 6.8], 2% SDS, and 10% glycerol) containing 1% complete mini protease inhibitor (Roche, Indianapolis, IN, USA) and phosphatase inhibitor cocktail (Thermo Fisher Scientific). Cell lysates were boiled (10 min at 98°C) and centrifuged (5 min at 16,000 × *g*) to eliminate insoluble cellular debris. Protein concentrations were determined using the BCA Protein Assay Kit (Thermo Fisher Scientific). 20 μg of protein extract was resolved by electrophoresis on an 8%–14% acrylamide gel and transferred to a PVDF membrane by standard methods. After blocking, membranes were incubated with anti-Ad5 capsid antibody (1:1,000; Abcam, Cambridge, UK, ab6982) (for capsid protein detection), anti-adenovirus-2/5 E1A [M73] (1:500; Santa Cruz Biotechnology, Dallas, TX, USA, Sc-25), anti-LC3B (1:500; Sigma-Aldrich, L7543), or anti-p62 (1:500; Abcam, ab109012). Protein labeling was detected using HRP-conjugated antibodies and visualized in the image reader LAS4000 (Fujifilm, Tokyo, Japan). Equal sample loading was confirmed by comparing the levels of glyceraldehyde-3-phosphate dehydrogenase (GAPDH).

Viral genome quantification

Cellular and viral DNA were obtained from infected cells or frozen tumors using Norgen's blood DNA isolation mini kit (Norgen Biotek, Thorold, CA, USA). Adenoviral genomes were analyzed by qPCR on a QuantStudio 7 Flex Real-Time PCR System (Thermo Fisher Scientific) using SYBR Green I Master Mix (Roche) as previously described.[21] The primers used are listed in Table S1.

Quantification of mRNA expression

Total and viral RNA were obtained from infected cells or frozen tumors using an RNeasy Mini Kit (Qiagen Iberia, Barcelona, Spain), 500 ng were reverse transcribed using the PrimeScript RT-PCR Kit (Takara Bio Europe, Saint-Germain-en-Laye, France), and the real-time qPCR reaction was performed using the LightCycler 480

SYBR Green I Master Mix (Roche). The results were normalized to the HPRT1 expression. The primers used are listed in Table S1.

RNA-seq

Total RNA was extracted using an RNeasy Mini Kit (Qiagen) following the manufacturer's recommendations. RNA integrity was examined with the TapeStation 4200 (Agilent, Santa Clara, CA, USA), and high-quality RNA samples were sequenced. For sequencing, the RNA-seq libraries were prepared according to the standard Illumina protocol with the Stranded mRNA Prep Ligation Kit and sequenced on a NextSeq 2000 sequencer (Illumina, San Diego, CA, USA).

RNA-seq processing and differential expression analysis

The transcript abundance was estimated using the quasi-mapping-based mode from the Salmon tool with the reference transcript from Ensemble (v.GRCh38) and the FASTQ files containing the reads.[39] The RNA-seq data counts obtained with Salmon were then analyzed using limma package v.3.6 available through the Bioconductor open source. The raw read counts were used as input to form a DGEList object combining the counts and associated annotations. Transcripts with at least 1 count per million (CPM) reads in all samples were kept. Scale normalization was applied, and the calculation of the normalized signal was performed by the voom function of the limma package. Differentially expressed genes (DEGs) between case and control samples were identified using the DESeq2 package in R.[40] DEGs were selected with $p < 0.05$ and $\log_2$ fold change (FC)| > 2. DEGs were visualized using a heatmap created with the R packages "ggplot2" and "pheatmap," respectively. The Venn diagram function from the limma R package was utilized to visualize the number of upregulated and downregulated genes that are either shared or exclusive to different case versus control DEGs.

Functional analysis

GSEA was run on the normalized dataset by comparing KPCI versus CMTI and KPCU versus CMTU using the gseGO function from the clusterProfiler R package.[41] DEGs were ranked according to a new metric calculated as sign(logFC)*−log10(p value), and this ranked list was used for the analysis. The Org.Mm.eg.db R package "Genome wide annotation for Mouse" v.3.8.2. was used to provide genome-wide annotation for the mouse reference genome. The Benjamini-Hochberg correction method was applied to adjust p values for multiple testing and control the false discovery rate (FDR). A p value cutoff of 0.05 was set for significance.

Antitumoral efficacy

Subcutaneous tumors were induced in the two flanks of athymic nude mice (ENVIGO, Indianapolis, IN, USA) or C57BL/6J mice (Charles River, Wilmington, MA, USA) by injecting 3×10^5 KPC-I cells in a ratio 1:1 with Matrigel. When tumors reached a volume of 40–50 mm^3, viruses were administered intravenously at 5×10^{10} vp/mouse in the athymic group (at 8 days post-inoculation) or intratumorally in each tumor (1×10^{11} vp/tumor) in immunocompetent mice as indicated in the scheme (at 15, 18, and 22 days post-inoculation) (Figure 6A). The tumor volume was calculated using the equation $V = 0.5 \times \text{length} \times \text{width}^2$. Animal procedures met the guidelines of European Community Directive 86/609/EEC and the local legislation (Decret 214/1997 of July 20 by the Department d'Agricultura, Ramaderia i Pesca de la Generalitat de Catalunya) under the approval of the Experimental Animal and Ethical Committee of the University of Barcelona (CEEA).

Viral progeny analysis from infected tumors

Tumors were mock treated or treated with AdNuPARE1A or ICOVIR15kDelE3, and cells were lysed in PBS by 3 rounds of freeze-thawing. After centrifugation, supernatants were used to infect A549 cells. After 4 h, viral and cellular DNA were obtained using Norgen's Blood DNA Isolation Mini Kit (Norgen Biotek), and viral genome quantification was performed as indicated.

Statistical analysis

Experimental data are represented by the mean ± SEM of at least four independent experiments. Statistical analysis was performed on GraphPad Prism v.8.0.1 (GraphPad Software). Statistical differences were evaluated using a two-tailed non-parametric Mann-Whitney test. The *in vivo* tumor growth statistical analysis was evaluated using R v.2.14.1 software with a linear mixed-effect model using the lme4 package. Statistical differences were evaluated using a multiple comparison of means by Tukey contrasts. In all cases, $p < 0.05$ was taken as the level of significance.

DATA AND CODE AVAILABILITY

Data are available within the published article and supplemental files. RNA-seq data are deposited at the European Nucleotide Archive (ENA) (https://www.ebi.ac.uk/ena/browser/view/PRJEB83822). Additional data are available from the corresponding author upon reasonable request.

ACKNOWLEDGMENTS

We are indebted to the Genomic Core, Flow Cytometry, and Biobank facilities of IDIBAPS for technical help and to the Unitat d'Experimentació Animal del Campus Clínic – CCiTUB for animal studies. This work was developed at the Centro Esther Koplowitz, Barcelona, Spain. M.O.-M. is the recipient of an iPFIS predoctoral contract from Instituto de Salud Carlos III (ISCIII), Spain. F.E.Jr. is the recipient of an FPI predoctoral contract from Spanish Ministerio de Ciencia e Innovación. This work was supported by grants to C.F. (PID2020-119692RB-C22 and PID2023-146637OB-C22) and R.A. (PID2020-119692RB-C21 and PID2023-146637OB-C21) from Spanish Ministerio de Ciencia e Innovación, with partial support from the Generalitat de Catalunya (SGR21/01169); ISCIII RICORS (RD21/0017/0012); AdenoNet RED2022-134221-T from Ministerio de Ciencia e Innovación; and the "la Caixa" Banking Foundation. CIBERER is an initiative of the ISCIII. We also acknowledge the support of CERCA Programme/Generalitat de Catalunya. Schemes and the graphical abstract were created with Biorender.com.

AUTHOR CONTRIBUTIONS

M.O.-M. designed and performed the experiments with adenovirus; F.E. contributed to the *in vivo* studies; S.A.-M. helped with the infectivity experiments; L.M.-B. helped with the *in vivo* experiments; G.C. and M.C. were responsible for the RNA-seq transcriptomic analysis; R.A. provided reagents and expertise and contributed to manuscript writing; and C.F. coordinated the study and wrote the manuscript.

DECLARATION OF INTERESTS

The authors declare no competing interests.

SUPPLEMENTAL INFORMATION

Supplemental information can be found online at https://doi.org/10.1016/j.omton.2024.200928.

REFERENCES

1. Zhao, Y., Liu, Z., Li, L., Wu, J., Zhang, H., Zhang, H., Lei, T., and Xu, B. (2021). Oncolytic Adenovirus: Prospects for Cancer Immunotherapy. Front. Microbiol. *12*, 707290. https://doi.org/10.3389/fmicb.2021.707290.
2. Lemos de Matos, A., Franco, L.S., and McFadden, G. (2020). Oncolytic Viruses and the Immune System: The Dynamic Duo. Mol. Ther. Methods Clin. Dev. *17*, 349–358. https://doi.org/10.1016/J.OMTM.2020.01.001.
3. Tollefson, A.E., Ying, B., Spencer, J.F., Sagartz, J.E., Wold, W.S.M., and Toth, K. (2017). Pathology in Permissive Syrian Hamsters after Infection with Species C Human Adenovirus (HAdV-C) Is the Result of Virus Replication: HAdV-C6 Replicates More and Causes More Pathology than HAdV-C5. J. Virol. *91*, e00284-17. https://doi.org/10.1128/JVI.00284-17.
4. Blair, G.E., Dixon, S.C., Griffiths, S.A., and Zajdel, M.E. (1989). Restricted replication of human adenovirus type 5 in mouse cell lines. Virus. Res. *14*, 339–346. https://doi.org/10.1016/0168-1702(89)90026-9.
5. Rincón, E., Cejalvo, T., Kanojia, D., Alfranca, A., Rodríguez-Milla, M.Á., Gil Hoyos, R.A., Han, Y., Zhang, L., Alemany, R., Lesniak, M.S., and García-Castro, J. (2017). Mesenchymal stem cell carriers enhance antitumor efficacy of oncolytic adenoviruses in an immunocompetent mouse model. Oncotarget *8*, 45415–45431. https://doi.org/10.18632/ONCOTARGET.17557.
6. González-Pastor, R., Ashshi, A.M., El-Shemi, A.G., Dmitriev, I.P., Kashentseva, E.A., Lu, Z.H., Goedegebuure, S.P., Podhajcer, O.L., and Curiel, D.T. (2019). Defining a murine ovarian cancer model for the evaluation of conditionally-replicative adenovirus (CRAd) virotherapy agents. J. Ovarian Res. *12*, 1–10. https://doi.org/10.1186/S13048-019-0493-5.
7. Zhang, L., Hedjran, F., Larson, C., Perez, G.L., and Reid, T. (2015). A novel immunocompetent murine model for replicating oncolytic adenoviral therapy. Cancer. Gene. Ther. *22*, 17–22. https://doi.org/10.1038/CGT.2014.64.
8. Halldén, G., Hill, R., Wang, Y., Anand, A., Liu, T.C., Lemoine, N.R., Francis, J., Hawkins, L., and Kirn, D. (2003). Novel immunocompetent murine tumor models for the assessment of replication-competent oncolytic adenovirus efficacy. Mol. Ther. *8*, 412–424. https://doi.org/10.1016/S1525-0016(03)00199-0.
9. Young, A.M., Archibald, K.M., Tookman, L.A., Pool, A., Dudek, K., Jones, C., Williams, S.L., Pirlo, K.J., Willis, A.E., Lockley, M., and McNeish, I.A. (2012). Failure of translation of human adenovirus mRNA in murine cancer cells can be partially overcome by L4-100K expression in vitro and in vivo. Mol. Ther. *20*, 1676–1688. https://doi.org/10.1038/MT.2012.116.
10. Sangrador, I., Molero, X., Campbell, F., Franch-Expósito, S., Rovira-Rigau, M., Samper, E., Domínguez-Fraile, M., Fillat, C., Castells, A., and Vaquero, E.C. (2018). Zeb1 in Stromal Myofibroblasts Promotes Kras-Driven Development of Pancreatic Cancer. Cancer. Res. *78*, 2624–2637. https://doi.org/10.1158/0008-5472.CAN-17-1882.
11. José, A., Rovira-Rigau, M., Luna, J., Giménez-Alejandre, M., Vaquero, E., García De La Torre, B., Andreu, D., Alemany, R., and Fillat, C. (2014). A genetic fiber modification to achieve matrix-metalloprotease-activated infectivity of oncolytic adenovirus. J. Control. Release. *192*, 148–156. https://doi.org/10.1016/J.JCONREL.2014.07.008.
12. Saito, K., Sakaguchi, M., Iioka, H., Matsui, M., Nakanishi, H., Huh, N.H., and Kondo, E. (2014). Coxsackie and adenovirus receptor is a critical regulator for the survival and growth of oral squamous carcinoma cells. Oncogene *33*, 1274–1286. https://doi.org/10.1038/ONC.2013.66.
13. Wang, H., Li, Z.Y., Liu, Y., Persson, J., Beyer, I., Möller, T., Koyuncu, D., Drescher, M.R., Strauss, R., Zhang, X.B., et al. (2011). Desmoglein 2 is a receptor for adenovirus serotypes 3, 7, 11 and 14. Nat. Med. *17*, 96–104. https://doi.org/10.1038/NM.2270.
14. Robertson, M.G., Eidenschink, B.B., Iguchi, E., Zakharkin, S.O., LaRocca, C.J., Tolosa, E.J., Truty, M.J., Jacobsen, K., Fernandez-Zapico, M.E., and Davydova, J. (2021). Cancer imaging and therapy utilizing a novel NIS-expressing adenovirus: The role of adenovirus death protein deletion. Mol. Ther. Oncolytics *20*, 659–668. https://doi.org/10.1016/J.OMTO.2021.03.002.
15. Brugada-Vilà, P., Cascante, A., Lázaro, M.Á., Castells-Sala, C., Fornaguera, C., Rovira-Rigau, M., Albertazzi, L., Borros, S., and Fillat, C. (2020). Oligopeptide-modified poly(beta-amino ester)s-coated AdNuPARmE1A: Boosting the efficacy of intravenously administered therapeutic adenoviruses. Theranostics *10*, 2744–2758. https://doi.org/10.7150/THNO.40902.
16. Jiang, H., White, E.J., Ríos-Vicil, C.I., Xu, J., Gomez-Manzano, C., and Fueyo, J. (2011). Human adenovirus type 5 induces cell lysis through autophagy and autophagy-triggered caspase activity. J. Virol. *85*, 4720–4729. https://doi.org/10.1128/JVI.02032-10.
17. Huch, M., Gros, A., José, A., González, J.R., Alemany, R., and Fillat, C. (2009). Urokinase-type plasminogen activator receptor transcriptionally controlled adenoviruses eradicate pancreatic tumors and liver metastasis in mouse models. Neoplasia *11*, 518–528. https://doi.org/10.1593/NEO.81674.
18. Mato-Berciano, A., Raimondi, G., Maliandi, M.V., Alemany, R., Montoliu, L., and Fillat, C. (2017). A NOTCH-sensitive uPAR-regulated oncolytic adenovirus effectively suppresses pancreatic tumor growth and triggers synergistic anticancer effects with gemcitabine and nab-paclitaxel. Oncotarget *8*, 22700–22715. https://doi.org/10.18632/ONCOTARGET.15169.
19. Bazan-Peregrino, M., Garcia-Carbonero, R., Laquente, B., Álvarez, R., Mato-Berciano, A., Gimenez-Alejandre, M., Morgado, S., Rodríguez-García, A., Maliandi, M.V., Riesco, M.C., et al. (2021). VCN-01 disrupts pancreatic cancer stroma and exerts antitumor effects. J. Immunother. Cancer *9*, e003254. https://doi.org/10.1136/JITC-2021-003254.
20. Rahib, L., Wehner, M.R., Matrisian, L.M., and Nead, K.T. (2021). Estimated Projection of US Cancer Incidence and Death to 2040. JAMA Netw. Open *4*, e214708. https://doi.org/10.1001/JAMANETWORKOPEN.2021.4708.
21. Rovira-Rigau, M., Raimondi, G., Marín, M.Á., Gironella, M., Alemany, R., and Fillat, C. (2019). Bioselection Reveals miR-99b and miR-485 as Enhancers of Adenoviral Oncolysis in Pancreatic Cancer. Mol. Ther. *27*, 230–243. https://doi.org/10.1016/J.YMTHE.2018.09.016.
22. Nisar, M., Paracha, R.Z., Adil, S., Qureshi, S.N., and Janjua, H.A. (2022). An Extensive Review on Preclinical and Clinical Trials of Oncolytic Viruses Therapy for Pancreatic Cancer. Front. Oncol. *12*, 875188. https://doi.org/10.3389/fonc.2022.875188.
23. Raimondi, G., Mato-Berciano, A., Pascual-Sabater, S., Rovira-Rigau, M., Cuatrecasas, M., Fondevila, C., Sánchez-Cabús, S., Begthel, H., Boj, S.F., Clevers, H., and Fillat, C. (2020). Patient-derived pancreatic tumour organoids identify therapeutic responses to oncolytic adenoviruses. EBioMedicine *56*, 102786. https://doi.org/10.1016/J.EBIOM.2020.102786.
24. Miyashita, N., Enokido, T., Horie, M., Fukuda, K., Urushiyama, H., Strell, C., Brunnström, H., Micke, P., Saito, A., and Nagase, T. (2021). TGF-β-mediated epithelial-mesenchymal transition and tumor-promoting effects in CMT64 cells are reflected in the transcriptomic signature of human lung adenocarcinoma. Sci. Rep. *11*, 22380. https://doi.org/10.1038/S41598-021-01799-X.
25. Liu, Y., Su, Z., Tavana, O., and Gu, W. (2024). Understanding the complexity of p53 in a new era of tumor suppression. Cancer. Cell. *42*, 946–967. https://doi.org/10.1016/J.CCELL.2024.04.009.
26. Chen, X., Cao, R., and Zhong, W. (2019). Host Calcium Channels and Pumps in Viral Infections. Cell *9*, 94. https://doi.org/10.3390/CELLS9010094.
27. Kondratskyi, A., Kondratska, K., Skryma, R., Klionsky, D.J., and Prevarskaya, N. (2018). Ion channels in the regulation of autophagy. Autophagy *14*, 3–21. https://doi.org/10.1080/15548627.2017.1384887.
28. Bootman, M.D., Chehab, T., Bultynck, G., Parys, J.B., and Rietdorf, K. (2018). The regulation of autophagy by calcium signals: Do we have a consensus? Cell. Calcium. *70*, 32–46. https://doi.org/10.1016/J.CECA.2017.08.005.
29. Gros, A., Puig, C., Guedan, S., Rojas, J.J., Alemany, R., and Cascallo, M. (2010). Verapamil enhances the antitumoral efficacy of oncolytic adenoviruses. Mol. Ther. *18*, 903–911. https://doi.org/10.1038/MT.2010.22.
30. Vervliet, T. (2018). Ryanodine receptors in autophagy: Implications for neurodegenerative diseases? Front. Cell. Neurosci. *12*, 89. https://doi.org/10.3389/fncel.2018.00089.
31. Bround, M.J., Wambolt, R., Luciani, D.S., Kulpa, J.E., Rodrigues, B., Brownsey, R.W., Allard, M.F., and Johnson, J.D. (2013). Cardiomyocyte ATP production, metabolic

flexibility, and survival require calcium flux through cardiac ryanodine receptors in vivo. J. Biol. Chem. *288*, 18975–18986. https://doi.org/10.1074/JBC.M112.427062.

32. Zhang, H., Knight, C., Chen, S.R.W., and Bezprozvanny, I. (2023). A Gating Mutation in Ryanodine Receptor Type 2 Rescues Phenotypes of Alzheimer's Disease Mouse Models by Upregulating Neuronal Autophagy. J. Neurosci. *43*, 1441–1454. https://doi.org/10.1523/JNEUROSCI.1820-22.2022.

33. Patergnani, S., Marchi, S., Rimessi, A., Bonora, M., Giorgi, C., Mehta, K.D., and Pinton, P. (2013). PRKCB/protein kinase C, beta and the mitochondrial axis as key regulators of autophagy. Autophagy *9*, 1367–1385. https://doi.org/10.4161/AUTO.25239.

34. Li, N., and Zhang, W. (2017). Protein kinase C β inhibits autophagy and sensitizes cervical cancer Hela cells to cisplatin. Biosci. Rep. *37*, BSR20160445. https://doi.org/10.1042/BSR20160445.

35. Kanaya, N., Kuroda, S., Kakiuchi, Y., Kumon, K., Tsumura, T., Hashimoto, M., Morihiro, T., Kubota, T., Aoyama, K., Kikuchi, S., et al. (2020). Immune Modulation by Telomerase-Specific Oncolytic Adenovirus Synergistically Enhances Antitumor Efficacy with Anti-PD1 Antibody. Mol. Ther. *28*, 794–804. https://doi.org/10.1016/J.YMTHE.2020.01.003.

36. Kudling, T.V., Clubb, J.H.A., Pakola, S., Quixabeira, D.C.A., Lähdeniemi, I.A.K., Heiniö, C., Arias, V., Havunen, R., Cervera-Carrascon, V., Santos, J.M., et al. (2023). Effective intravenous delivery of adenovirus armed with TNFα and IL-2 improves anti-PD-1 checkpoint blockade in non-small cell lung cancer. OncoImmunology *12*, 2241710. https://doi.org/10.1080/2162402X.2023.2241710.

37. Rojas, J.J., Gimenez-Alejandre, M., Gil-Hoyos, R., Cascallo, M., and Alemany, R. (2012). Improved systemic antitumor therapy with oncolytic adenoviruses by replacing the fiber shaft HSG-binding domain with RGD. Gene. Ther. *19*, 453–457. https://doi.org/10.1038/GT.2011.106.

38. Villanueva, E., Martí-Solano, M., and Fillat, C. (2016). Codon optimization of the adenoviral fiber negatively impacts structural protein expression and viral fitness. Sci. Rep. *6*, 27546. https://doi.org/10.1038/SREP27546.

39. Patro, R., Duggal, G., Love, M.I., Irizarry, R.A., and Kingsford, C. (2017). Salmon provides fast and bias-aware quantification of transcript expression. Nat. Methods *14*, 417–419. https://doi.org/10.1038/NMETH.4197.

40. Love, M.I., Huber, W., and Anders, S. (2014). Moderated estimation of fold change and dispersion for RNA-seq data with DESeq2. Genome. Biol. *15*, 550. https://doi.org/10.1186/S13059-014-0550-8.

41. Wu, T., Hu, E., Xu, S., Chen, M., Guo, P., Dai, Z., Feng, T., Zhou, L., Tang, W., Zhan, L., et al. (2021). clusterProfiler 4.0: A universal enrichment tool for interpreting omics data. Innovations *2*, 100141. https://doi.org/10.1016/J.XINN.2021.100141.